On the Measurement of Shock Waves

KEVIN J. PARKER, MEMBER, IEEE, AND E. M. FRIETS

Abstract—**The classic theoretical formulations of finite-amplitude distortion invariably depict continuous sinusoidal waves which develop into sawtooth or N-shaped waves. In practice, where ultrasonic waveforms at high intensities are measured by a PVDF hydrophone connected to an oscilloscope, waveforms are observed with gross asymmetries between positive and negative pressure amplitudes, high-amplitude spikes, notches, ringing, and other peculiarities. In principle, additional nonlinearities in the driving stages or the receiving system may influence the observed waveform. However, it is not necessary to invoke nonlinearities in the transmit or receive systems to explain the time-domain appearance of many waveforms. Instead, linear mechanisms exist which affect the waveshape. The first is a relative phase shift betwen the fundamental and second (and higher) harmonics which occurs in a diffraction-limited focused field. This alters the time-domain appearance but not the spectral content of the observed signal. The second class of linear mechanisms involves hydrophone cable and impedance mismatch effects which alter both time- and frequency-domain characteristics of the actual pressure waveform incident on the hydrophone. These effects and others are illustrated. The results form the basis for some recommendations on experimental procedures in nonlinear wave propagation.**

INTRODUCTION

NONLINEAR acoustics has a history dating back to the previous century [1] and more recently has been actively developed in underwater acoustics [1]–[9]. However, specific publications on finite-amplitude distortion in medical ultrasonics were infrequent until the works of Carstensen, Muir, and collaborators [10]–[12] in the early 1980's. Since then, a range of issues has been considered, including the effects of finite-amplitude distortion on heating and lesion production in biological tissue [12]–[14], the generation of shock from medical ultrasonic equipment [15]–[17], and the measurement of B/A for tissue characterization or imaging [18], [19].

One potential source of experimental difficulties in the area of nonlinear acoustics at biomedical frequencies (1–12 MHz) is the discrepency between the classic description of the sawtooth or N-shock wave and the actual waveshape observed using broad-band PVDF hydrophones. Beam profiles and calibration procedures are particularly complicated by waveforms (broad or narrow band) which exhibit gross asymmetries between positive and negative cycles, high-amplitude spikes or peaks, or other features such as notches or ringing. Some speculation has centered on possible nonlinearities in PVDF hydrophones as a cause of waveform artifacts [20], but the evidence [21]–[23] indicates hydrophone fidelity well above 10^3 W/cm^2. Clearly, the linear and nonlinear characteristics of three basic components (source electronics transducer, fluid medium, and hydrophone amplifier display) must be evaluated as a prerequisite for investigations of nonlinear acoustics.

This paper attempts to systematically cover some phenomena which account for "anomalous" waveshapes. It is shown that linear mechanisms explain some major discrepencies between classic sawtooth waves and those typically recorded. The results suggest some guidelines for experimental procedures.

THEORY

A shock parameter σ, which characterizes the growth and dissipation of harmonics, has been formulated for ideal plane and spherical waves [3], [10]. The shock parameter is proportional to frequency, source velocity, and some measure of propagation distance. Benchmarks for weak and hard shock are $\sigma = 1$ and 3, respectively, and hard shock is characterized by the time-domain appearance of sawtooth or N-shaped waves with a discontinuity between equal magnitude compression and rarefaction peaks. Illustrations of these important and fundamental concepts have appeared in many references [1], [3], [6], [10], [16]. The early formulations do not deal with additional complexities of beam diffraction effects in near-field or focused-field regions. Recently, derivations have been proposed which utilize a description of the primary field based on a parabolic approximation of the Helmholtz wave equation. Combined with other approximations, the effects of both beam diffraction and finite-amplitude distortion can be modeled [7], [8], [24], [25] for the case of weak shock ($\sigma < 1$). In particular, Lucas and Muir [7] described the magnitude and phase of the second harmonic in a focused system where the F number (ratio of focal length to aperture diameter) was equal to two. Phase shifting in the focal region differed from the case of linear radiation, and the relative phase shift between the fundamental and second harmonic was shown to be the important determinant of waveshape. Other treatments of phase shifts in focused nonlinear fields are found in works by Sutin [26] and Rugar [27].

Manuscript received April 25, 1986; revised September 23, 1986. This work was supported in part by the Whitaker Foundation, NSF Grant ECE-8415253, and NIH Grant CA-39241-23.

K. J. Parker is with the Department of Electrical Engineering, University of Rochester, Rochester, NY 14627.

E. M. Friets was with the Department of Electrical Engineering, University of Rochester, Rochester, NY. He is now with the Thayer School of Engineering, Dartmouth College, Hanover, NH 03766.

IEEE Log Number 8612863.

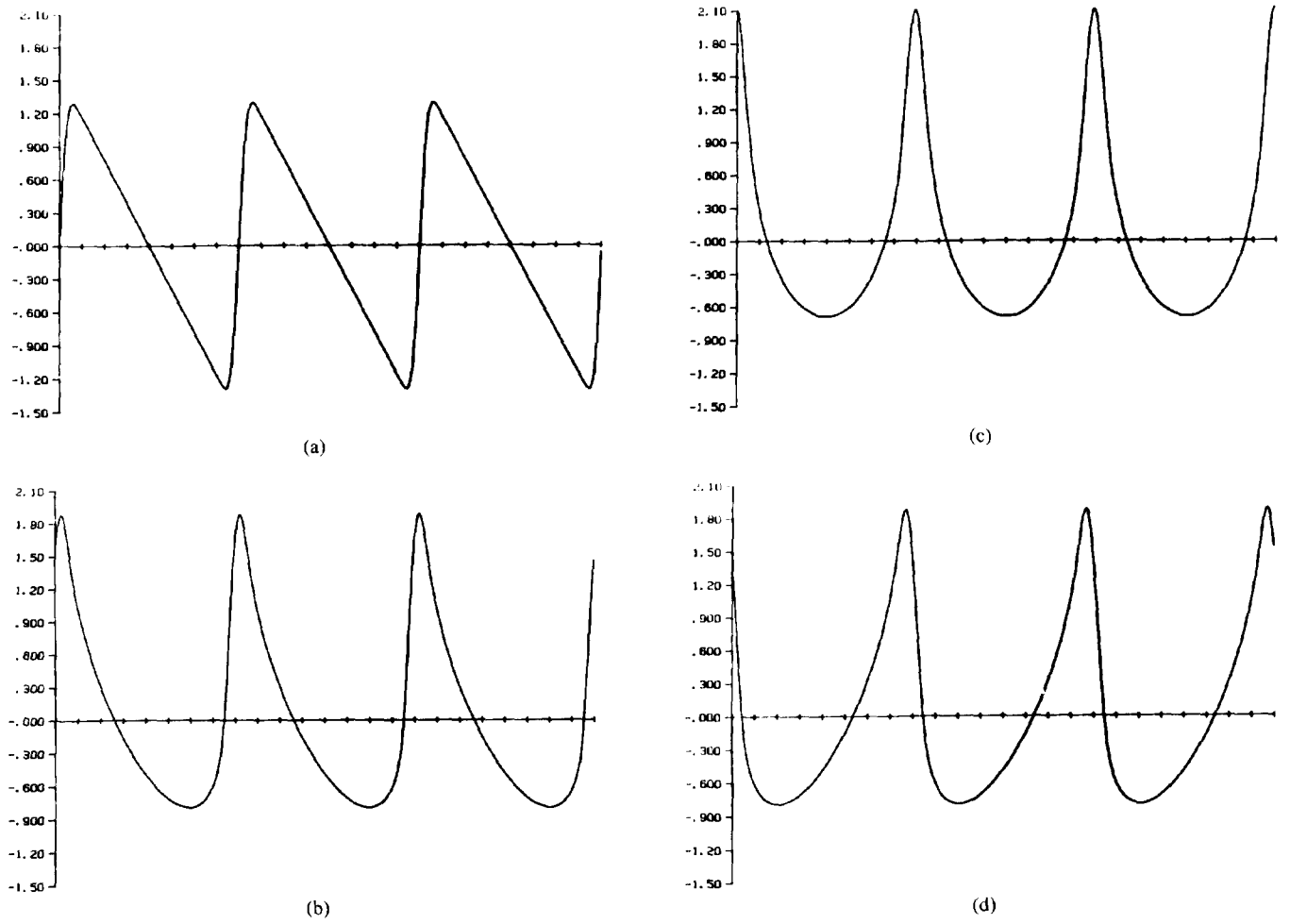

Fig. 1. Family of curves representing sawtooth wave with progressively increasing phase shift between harmonics. Phase shift ϕ is 0 in (a), $\pi/4$ in (b), $\pi/2$ in (c), and $3/4\pi$ in (d). These are representative of waveforms measured in focused fields.

Results and Discussion

A. Phase Shifts

This section investigates the effects of relative phase shifts between the first ten harmonics of fully developed shock. The Fourier components of a symmetric sawtooth or N wave are given by

$$f(t) = A \sum_{n=1}^{\infty} \frac{1}{n} \sin (n\omega t). \tag{1}$$

Lucas and Muir [7] introduced a position-dependent phase shift ϕ between the fundamental and second harmonic. For the purposes of illustration, we simply extend the phase shift ϕ to all harmonics such that a wave in hard shock can be described at any fixed position by the series

$$g(t) = A \sum_{n=1}^{\infty} \frac{1}{n} \sin (n\omega t + \phi). \tag{2}$$

This is, of course, distinct from phase linear argument of the kind $n(\omega t + \theta)$ which would correspond to a simple time-axis shift of the waveform. While the constant phase term of (2) does not change the magnitude of the waveform Fourier components, the effect in the time domain is to generate asymmetric positive and negative cycles. The effect is shown in Fig. 1, where plots of (2) are given for different values of ϕ. Three cycles each are shown of waveforms with arbitrary but uniform amplitude A. Only ten harmonics were used in these graphs, and some additional smoothing in the time domain (weak low-pass filtering in the frequency domain) was performed to eliminate residual Gibbs phenomenon and fluctuations caused by abrupt truncation of the Fourier series. As the phase shift ϕ is incremented from zero to $(3/4)\ \pi$, the ratio of positive to negative peaks increases from 1 : 1 to approximately 3 : 1. A phase shift of $\phi = \pi$ (not shown) produces a reversed or mirror image of the original sawtooth ($\phi = 0$). In general, as more harmonics are added, the sharpness and height of the positive peak is enhanced.

In experimental beam plots the relative phase shift between harmonics will be a strong function of positive in focal regions [7], [26], [27]. Depending on applications, for example, cavitation research or lesion production, the important parameter may be either peak pressure, peak-to-peak pressure, time-averaged values of magnitude of pressure or pressure squared, or the magnitude square of each harmonic. The relationship between these different measures will change as ϕ is varied, complicating some calibration procedures. However, other mechanisms may

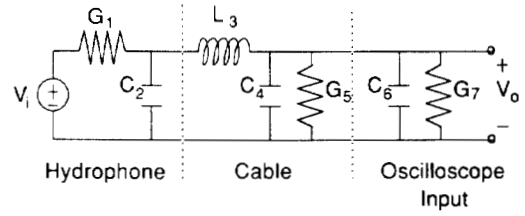

Fig. 2. Simple lumped-parameter model for hydrophone, cable, and oscilloscope amplifier termination.

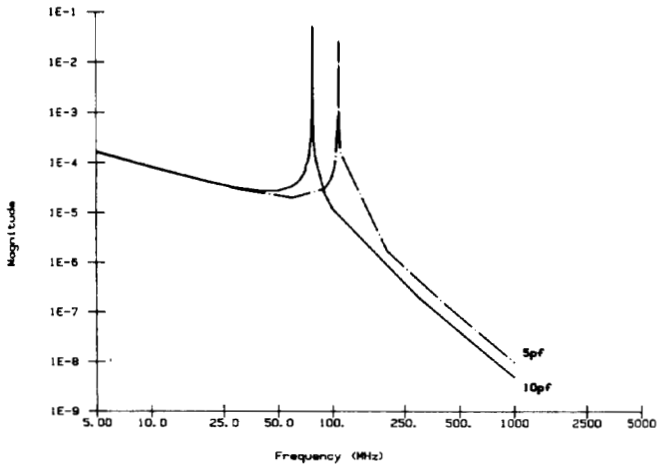

Fig. 3. Magnitude of voltage output to input for simple lumped-parameter model of minature hydrophones (5- and 10-pF probe capacitance shown) connected to 1.5 m of 50-Ω cable terminated at high-impedance oscilloscope amplifier. Strong resonance is predicted which can be excited by harmonic-rich shock waveforms.

also introduce phase shifts, as discussed in the next sections.

B. Cable Lumped-Parameter Model

A crude yet useful model of hydrophone and coaxial cable with discrete or lumped-parameter RLC values and termination on a high-impedance oscilloscope amplifier input is shown in Fig. 2. The transfer function between voltage input V_i and output V_o is obtained from circuit analysis:

$$\frac{V_o(s)}{V_i(s)} = \frac{G_1}{s^3(C_9L_3C_2) + s^2(C_2L_3G_8 + G_1L_3C_9) + s(C_9 + C_2 + L_3G_1G_8) + (G_1 + G_8)} \tag{3}$$

where s is the Laplace transform variable, $C_9 = C_4 + C_6$, and $G_8 = G_5 + G_7$. For typical parameter values we estimate for a 1-mm PVDF element: $G_1 = 1 \times 10^{-6}$ mho, $C_2 = 5 \times 10^{-12}$ F. Cable lumped-parameter values are approximately $L_3 = 0.3 \times 10^{-6}$ H/m, $C_4 = 110 \times 10^{-12}$ F/m, $G_5 = 6 \times 10^{-6}$ mho/m, for 50-Ω coaxial cable [28] such as RG58. For the termination, $C_6 = 20 \times 10^{-12}$ F and $G_7 = 1 \times 10^{-6}$ mho are representative values. The denominator of (3) includes two complex conjugate poles $s = -a \pm jb$ where $|b| >> |a|$ for the parameter values listed previously. Effectively, lengths of cable on the order of 1 m add sufficient inductance to create resonant behavior. For example, using the foregoing values and assuming 1.5 m of cable, the transfer function corresponds to a high Q system resonant at 107 MHz. For longer cable lengths or higher capacitance probes the resonant frequency shifts downward towards 77 MHz for a 1.5-m cable with a 10-pF hydrophone element. Transfer functions are shown in Fig. 3 for the 1.5-m cable with 5- and 10-pF elements. The curves show the nonuniform gain and also demonstrate the sensitivity of the resonance frequency to the hydrophone capacitance.

If signals are restricted to the low MHz band, the magnitude and phase of the transfer function of the model circuit are relatively flat or can be calibrated, enabling accurate waveform reproduction. However, assuming a wave in hard shock, the higher harmonics may be differentially transmitted and phase shifted compared to the fundamental and lower harmonics. In addition, the higher harmonics can excite resonance behavior of the circuit. As an example, Fig. 4(a) shows a recorded waveform obtained in the focused field of continuous 3.4-MHz radiation (8-cm focal length, 2.5-cm diameter ceramic source). A 1-mm needle-type PVDF hydrophone was utilized with its 75-Ω cable connected directly to the input of a digitizing oscilloscope. The horizontal scale is 200 ns/100 samples, with arbitrary vertical scale. Fig. 4(a) is the waveform with $0.5 < \sigma < 1$ near the focal region. A slight asymmetry is evident between positive and negative peaks. Fig. 4(b) is the same wave with $1 < \sigma < 2$, and the asymmetry is more pronounced with a narrow positive going peak. The source output is again increased so that approximately $2 < \sigma < 3$ in Fig. 4(c). A strong positive peak followed by a notch is evident. However, these could be linear superpositions of a waveform such as in Fig. 4(b) or Fig. 1, plus an impulsive-type response of a damped resonant circuit above 20 MHz. That this resonance may be attributable to the cable and not the PVDF element is suggested by Fig. 4(d), where source output is the same as in Fig. 4(c) but an extension cable of approximately 1-m RG58 cable has been added between the hydrophone and oscilloscope. The presence of a higher frequency resonance is quite evident in this case. These results are in agreement with the observations of Bacon [21] and Shombert and Harris [23] concerning the causes of high-frequency oscillations which follow the shock edge.

C. Transmission Line Effects

Impedance mismatches between cables and terminations or elements will modify broad-band waveforms. Although cable lengths are typically much shorter than wavelengths of E-M signals below 30 MHz, and one would not expect to measure variable transmission line voltages as a function of position, a frequency-dependent transfer function may still exist. For a transmission line of impedance Z_o Ω with a wave of voltage V_o incident on

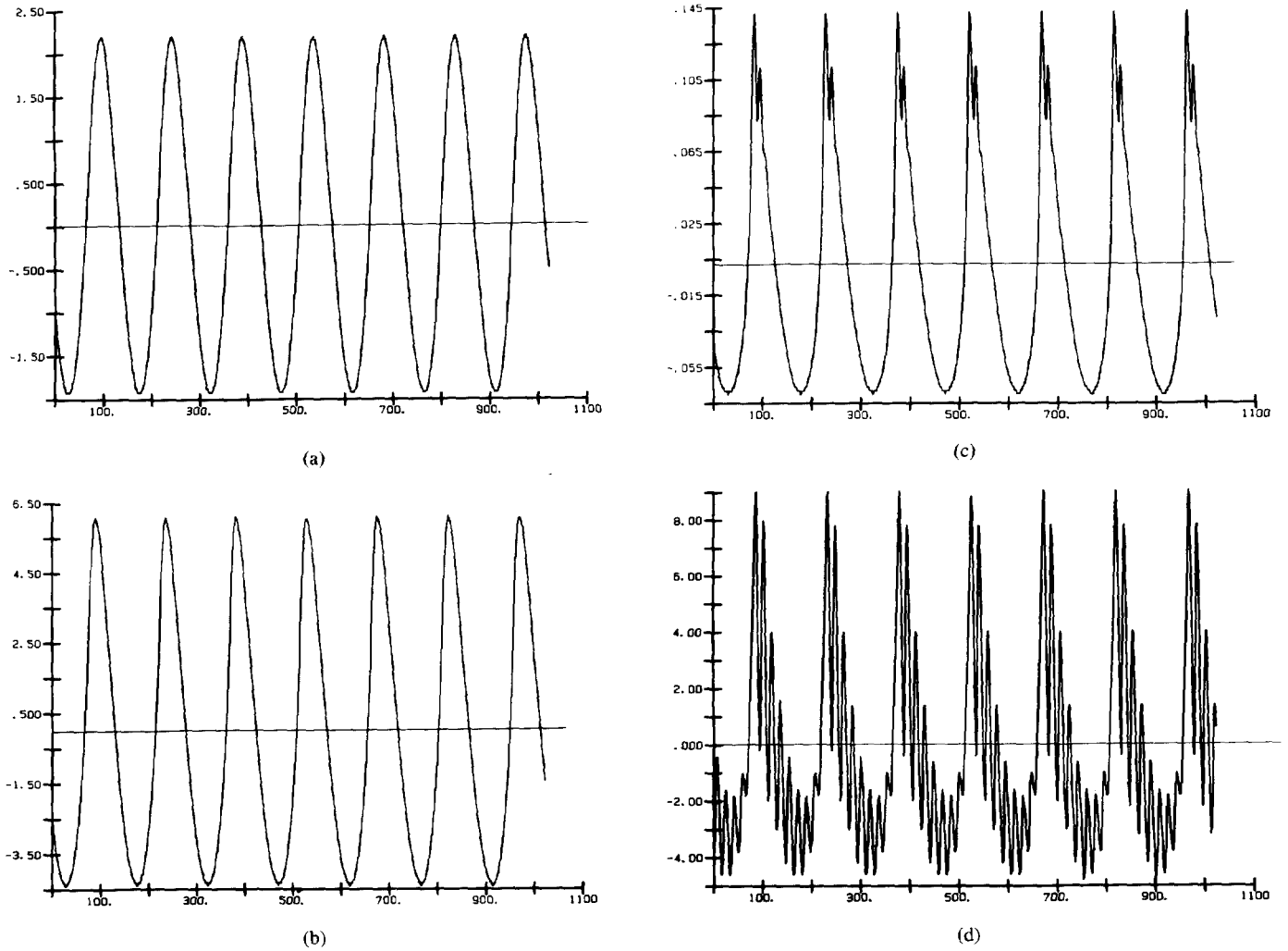

Fig. 4. Measured waveforms from 3.4-MHz focused beam obtained at increasing values of shock parameter σ. Power output was adjusted so that shock parameter was approximately 0.5, 1.5, 2.5, and 2.5 in (a), (b), (c), and (d), respectively. In (d) coaxial cable length has been added between hydrophone and oscilloscope, increasing net inductance of circuit.

a discrete termination $Z_L(j\omega)$, the total voltage $\hat{V}$ (incident plus reflected) at positions close to the termination is given simply by [28]

$$\frac{\hat{V}}{V_o} = \left(\frac{2Z_L(j\omega)}{Z_L(j\omega) + Z_o}\right). \tag{4}$$

Thus the transfer function is governed by the termination frequency dependence.

Impedance mismatches can also be determined using time-domain reflection where the corresponding frequency-domain transfer functions may be derived by the Fourier transform of the impulse response. A set of impulse response experiments were performed to illustrate these effects. A 5-ns pulse generator and oscilloscope were T connected to a long transmission line (5 m of RG58, 50-Ω coaxial) as shown in Fig. 5. The length is more than typically required in laboratory experiments but was necessary for adequate separation of echoes. The transmission line was connected to either a nominally 50-Ω RF termination (Fig. 6(a)), a 0.5-m length of 75-Ω cable terminated with discrete a 1-MΩ resistor and 100-pF capacitor (Fig. 6(b)), a 1-mm needle-type PVDF hydrophone (Fig. 6(c)), or finally, a 1-mm spot-poled membrane PVDF hydrophone (Fig. 6(d)). The digitized waveforms had a 50-ns/100-sample sweep, with the vertical axis in volts. In each figure the first peak (sample 100) is the transmitted impulse, the second (samples 200–300) the reflected impulse from the termination, and subsequent echoes are multiple reverberations. The echoes demonstrate that the 50-Ω RF terminator was a reasonable, albeit not perfect, impedance match given the small amplitude reflection. Some pulse widening is expected given nonzero attenuation and dispersion. The 75-Ω cable length

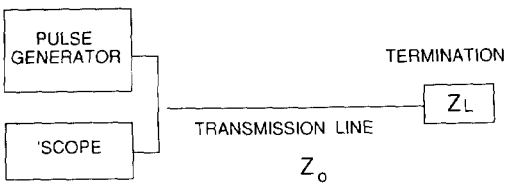

Fig. 5. Experimental configuration for time-domain reflections of pulses from impedance mismatch of load and transmission line.

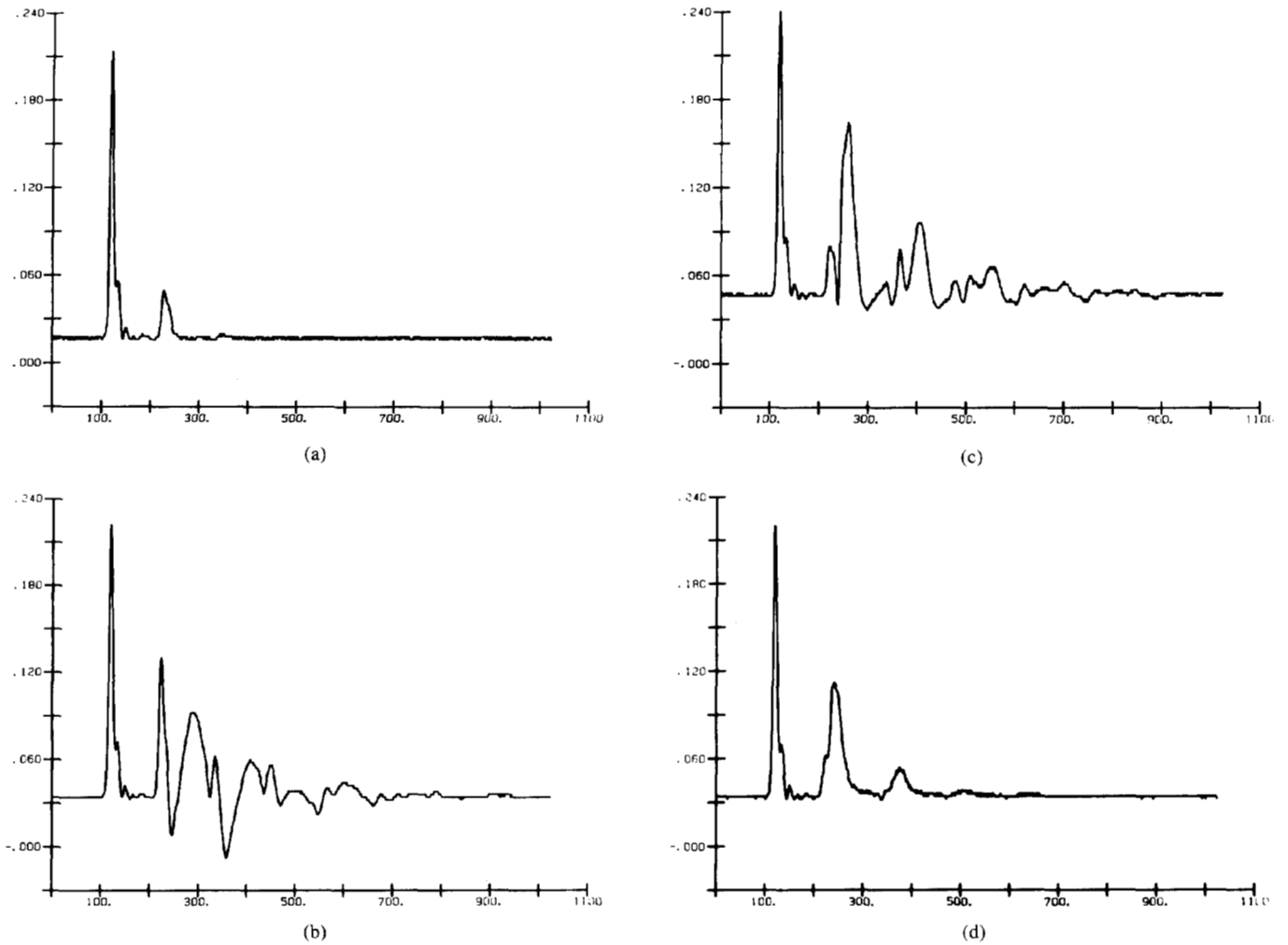

Fig. 6. Time domain reflections of 5-ns pulse propagating along 5-m coaxial cable. Terminations are (a) 50-Ω RF attenuator; (b) short 75-Ω cable with RC termination; (c) PVDF needle hydrophone; (d) PVDF spot-poled hydrophone.

with RC termination (a crude model of PVDF hydrophones) shows large pulse distortion and reflection as expected. The needle probe displays similar characteristics while the spot-poled probe reflection is qualitatively closest to the 50-Ω RF terminator.

In actual experiments these time-domain reflections would not be observed directly because of shorter cable lengths, slower sweep rates, and different exitation sources and waveforms. However, time-domain distortion of an impulse directly implies frequency-dependent transfer functions. Thus a harmonic-rich input signal will not be reproduced with fidelity. In practice, the termination mismatch effects can be minimized by a preamplifier on or very close to the PVDF probe, with appropriately chosen input and output impedances [21], [23]. In addition, the lumped-parameter cable inductance effects would be greatly diminished by using a 50-Ω termination at the oscilloscope, a situation only permissible given a 50-Ω output impedance preamplifier.

D. Source Considerations

The spectral purity of a CW waveform is highly dependent upon electronics and components used. Harmonics 30 dB below fundamental are common for many analog and synthesized RF sources. Power amplifier nonlinearities will generally add to the harmonics, and gating circuits, particularly doubly balanced mixers used for tone burst windowing, are notoriously capable of generating harmonics. To demonstrate the effects of distortion in the source electronics, we compare the waveforms generated using sine- and square-wave sources of the same amplitude and fundamental frequency. Square waves are composed of odd harmonics, which suits the output characteristics of the narrow-band ceramic transducer employed in these experiments. Furthermore, square-wave excitation of the transducer is an extreme example of distortion (clipping) in the electronics. Fig. 7(a) and (b) show the waveforms recorded from a 1-mm needle-type PVDF hydrophone in the focus of a 2.39-MHz field (8-cm focal length, 2.5-cm-diameter ceramic source). The hydrophone cable is directly connected to a digitizing oscilloscope with 500-ns/100-sample sweep rate and uncalibrated but constant vertical axis. In both cases a tone burst of four cycles, 2.39 MHz, is delivered to the source at low power levels ($\sigma \ll 1$). Fig. 7(a) shows typical rise and ring-down for the narrow-band source transducer.

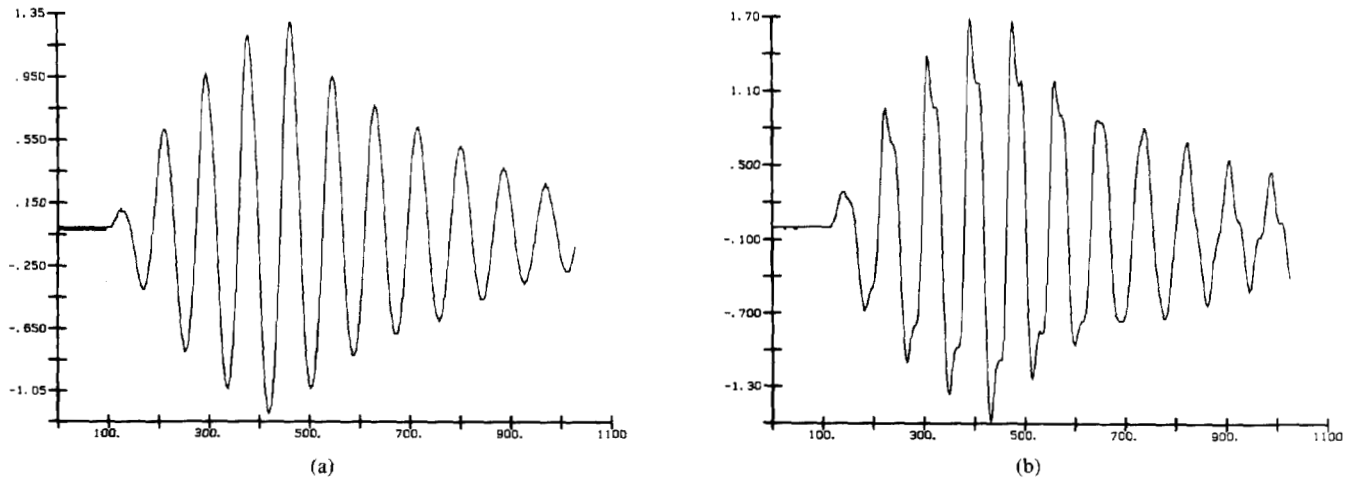

Fig. 7. Measured 2.39-MHz waveforms in focused field. (a) Four-cycle sine-wave tone burst is used as excitation. (b) Four-cycle square wave employed to represent clipping or distortion of input signal.

Fig. 7(b) shows the results of square-wave excitation. Actual square waves are not seen because of frequency-dependent transfer functions in the source amplifier and transmitter, the fluid, and the receiving system. The result is spikes or peaks on the forced waveforms (first four cycles) and an intermodulation pattern on the ring-down or unforced cycles as the source transducer harmonics decay at individual rates and relative phase shifts.

Note that narrow-band air-backed sources are quite capable of radiating even harmonics although at much reduced efficiency from the fundamental and odd harmonics. Thus the spectral purity of source excitation must be evaluated in experimental work by sampling the RF power amplifier output near the transducer and also by hydrophone measurements of pressure waveforms at the acoustic source. It is especially important that these procedures be included in studies of harmonic-rich signals in biological tissue, where issues of heating and bioffects require discrimination between linear and nonlinear propagation modes.

Conclusion

The physics of finite-amplitude distortion in the presence of beam diffraction effects entails position-dependent phase shifts between the fundamental and harmonics. One family of curves resulting from the simple phase relation of (2) was shown in Fig. 1(a)–(d), and these simulations bear close relationship to measured waveforms. Other phase relations may be formulated or measured, but one generalization is that measured parameters such as peak-to-peak voltage (pressure) or peak-positive voltage are critically dependent on phase relations. Thus linear transfer function characteristics of the probe–cable–oscilloscope chain require evaluation. The cable inductance under certain circumstances can lead to a spike and notch pattern on the sharp edge of a wave in hard shock. Ideally, a close proximity hydrophone preamplifier with matched input and 50-Ω output impedances, connected to 50-Ω coaxial cable and a 50-Ω RF attenuator at the oscilloscope input, would alleviate problems with system impedance mismatches and cable inductance. Finally, nonlinearities (other than the fluid B/A) are more likely found in the transmit chain as opposed to the receiving PVDF element. The spectral purity of power RF lines and the radiation at the transducer require prior measurement to distinguish between linear superposition of transmitted fields and true harmonic generation from fluid nonlinearities.

Acknowledgment

Helpful discussions with Prof. E. L. Carstensen and Dr. G. A. Harris are gratefully acknowledged. Thanks are also extended to Prof. T. Muir and Prof. D. Blackstock for their insightful comments on general nonliner acoustics.

References

[1] R. T. Beyer, Ed., *Nonlinear Acoustics in Fluids*. New York: Van Nostrand-Reinhold, 1984.

[2] D. T. Blackstock, "On plane, spherical, and cylindrical sound waves of finite amplitude in lossless fluids," *J. Acoust. Soc. Amer.*, vol. 36, pp. 217–219, 1964.

[3] ——, "Connection between the Fay and Fubini solutions for plane sound waves of finite amplitude," *J. Acoust. Soc. Amer.*, vol. 39, pp. 1019–1026, 1966.

[4] J. C. Lockwood, T. G. Muir, and D. T. Blackstock, "Directive harmonic generation in the radiation field of a circular piston," *J. Acoust. Soc. Amer.*, vol. 53, pp. 1148–1153, 1973.

[5] L. Bjorno, Ed., "Finite amplitude wave effects in fluids," in *Proc. 1973 Symp.*, IPC Science and Tech. Press, LTD, 1984.

[6] J. A. Shooter, T. G. Muir, and D. T. Blackstock, "Acoustic saturation of spherical waves in water," *J. Acoust. Soc. Amer.*, vol. 55, pp. 54–62, 1974.

[7] B. G. Lucas and T. G. Muir, "Field of a finite-amplitude focusing source," *J. Acoust. Soc. Amer.*, vol. 74, no. 5, 1983.

[8] M. F. Hamilton, J. N. Tjøtta, and S. Tjotta, "Nonlinear effects in the farfield of a directive sound source," *J. Acoust. Soc. Amer.*, vol. 78, no. 1, 1985.

[9] D. T. Blackstock, "Generalized Burgers equation for plane waves," *J. Acoust. Soc. Amer.*, vol. 77, no. 6, 1985.

[10] T. G. Muir and E. L. Carstensen, "Prediction of nonlinear acoustic effects at biomedical frequencies and intensities," *Ultrasound Med. Biol.*, vol. 6, pp. 345–357, 1980.

[11] E. L. Carstensen, W. K. Law, N. D. McKay, and T. G. Muir, "Demonstration on nonlinear acoustical effects at biomedical frequencies and intensities," *Ultrasound Med. Biol.*, vol. 6, pp. 359–368, 1980.

[12] E. L. Carstensen, S. A. Becroft, W. K. Law, and D. B. Barbee, "Finite amplitude effects on the thresholds for lesion production in

tissues by unfocused ultrasound," *J. Acoust. Soc. Amer.*, vol. 70, no. 2, 1981.
[13] M. E. Haran and B. D. Cook, "Distortion of finite amplitude ultrasound in lossy media," *J. Acoust. Soc. Amer.*, vol. 73, no. 3, 1983.
[14] W. Swindell, "A theoretical study of nonlinear effects with focused ultrasound in tissues: An 'acoustic Bragg peak,'" *Ultrasound Med. Biol.*, vol. 11, pp. 121–130, 1985.
[15] K. J. Parker, "Observation of nonlinear acoustic effects in a B-scan imaging instrument," *IEEE Trans. Sonics Ultrason.*, vol. SU-30, pp. 4–8, 1985.
[16] D. R. Bacon, "Finite amplitude distortion of the pulsed fields used in diagnostic ultrasound," *Ultrasound Med. Biol.*, vol. 10, pp. 189–195, 1984.
[17] H. C. Starritt, M. A. Perkins, F. A. Duck, and V. F. Humphrey, "Evidence for ultrasonic finite-amplitude distortion in muscle using medical equipment," *J. Acoust. Soc. Amer.*, vol. 77, no. 1, 1985.
[18] F. Dunn, W. K. Law, and L. A. Frizzell, "Nonlinear ultrasonic wave propagation in biological materials," in *Proc. IEEE Ultrasonics Symp.*, 81CH1689-9, 1981, pp. 527–532.
[19] N. Ichida, T. Sato, and M. Linzer, "Imaging the nonlinear ultrasonic parameter of a medium," *Ultrasonic Imaging*, vol. 5, pp. 295–299, 1983.
[20] G. Kossoff and D. A. Carpenter, "A reflection technique for measurement of high acoustic intensities," *Ultrasound Med. Biol.*, vol. 10, pp. 197–199, 1984.
[21] D. A. Bacon, "Characteristics of a PVDF membrane hydrophone for use in the range 1–100 MHz," *IEEE Trans. Sonics Ultrason.*, vol. SU-29, pp. 18–25, 1982.
[22] D. A. Bacon, "The observation of distorted waveforms," *Ultrasound Med. Biol.*, vol. 10, pp. 639–640, 1984.
[23] O. G. Shombert and G. R. Harris, "Use of miniature hydrophones to determine peak intensities typical of medical ultrasound devices," *IEEE Trans. Ultrasonics, Ferroelectrics, Frequency Contr.*, vol. UFFC-33, pp. 287–294, 1986.
[24] S. I. Aanonsen, T. Barkve, J. N. Tjotta, and S. Tjotta, "Distortion and harmonic generation in the nearfield of a finite amplitude sound beam," *J. Acoust. Soc. Amer.*, vol. 75, no. 3, 1984.
[25] G. Du and M. A. Breazeale, "Theoretical description of a focused Gaussian beam," *J. Acoust. Soc. Amer.*, Supplement 1, vol. 78, p. S 39 (abstract), 1985.
[26] A. M. Sutin, "Influence of nonlinear effects on the properties of acoustic focusing systems," *Soc. Phys. Acoust.*, vol. 24, pp. 334–339, 1978.
[27] D. Rugar, "Resolution beyond the diffraction limit in the acoustic microscope: A nonlinear effect," *J. Appl. Phys.*, vol. 56, pp. 1338–1346, 1984.
[28] J. D. Kraus and K. R. Carver, *Electromagnetics*. New York: McGraw-Hill, 1973, ch. 13.

Kevin J. Parker (S'79–M'81) was born in Rochester, NY, in 1954. He received the B.S. degree in engineering science, *summa cum laude*, from the State University of New York, Buffalo, in 1976, and the M.S. and Ph.D. degrees in electrical engineering, specializing in biomedical ultrasonics, from The Massachusetts Institute of Technology, Cambridge, in 1978 and 1981, respectively.

From 1981 to 1985 he was an Assistant Professor of Electrical Engineering at the University of Rochester, Rochester NY; currently he holds the title of Associate Professor. His research interests are in ultrasonic tissue characterization, medical imaging, and general linear and nonlinear acoustics.

Dr. Parker was the recipient of a National Institute of General Medical Sciences Biomedical Engineering Fellowship (1979), Lilly Teaching Fellowship (1982), and Whitaker Foundation Biomedical Engineering Grant Award (1983). He serves as Chairman of the Rochester Section of the IEEE Engineering in Medicine and Biology Society, a member of the IEEE Sonics and Ultrasonics Symposium Technical Committee, and as reviewer and consultant for a number of journals and institutions. He is also a member of the Acoustical Society of America, and the American Institute of Ultrasound in Medicine.

E. M. Friets was born on Staten Island, NY, in 1963. He received the B.S. degree from the University of Rochester, Rochester, NY, in 1985, and is currently working toward the Ph.D. degree in biomedical engineering at Dartmouth College, Hanover, NH. His current research interests include medical imaging and a frameless stereotactic procedure for neurosurgery.